Dicer-like 5 deficiency confers temperature-sensitive male sterility in maize

Authors: Chong Teng[1†], Han Zhang[2†], Reza Hammond[3], Kun Huang[3], Blake C. Meyers[1,4*], Virginia Walbot[2*]

Affiliations:

[1]Donald Danforth Plant Science Center, 975 N. Warson Rd, St. Louis, MO 63132, USA.

[2]Department of Biology, Stanford University, Stanford, CA 94305, USA.

[3]Delaware Biotechnology Institute, University of Delaware, Newark, DE 19716, USA.

[4]University of Missouri – Columbia, Division of Plant Sciences, 52 Agriculture Lab, Columbia, MO 65211, USA.

[*]**Correspondence to: walbot@stanford.edu (V.W.); bmeyers@danforthcenter.org (B.C.M.)**

[†]These authors contributed equally to this work.

Abstract

Small RNAs play important roles during plant development by regulating transcript levels of target mRNAs, maintaining genome integrity, and reinforcing DNA methylation. *Dicer-like 5* (*Dcl5*) is proposed to be responsible for precise slicing to generate diverse 24-nt phased, secondary small interfering RNAs (phasiRNAs), which are exceptionally abundant in meiotic anthers of maize, rice, and other grasses [1]. The importance and functions of these phasiRNAs remain unclear. Here, we used the Clustered Regularly Interspaced Short Palindromic Repeats (CRISPR) *Cas9* system to mutate *Dcl5*. We report that *dcl5* mutants have few or no 24-nt phasiRNAs, develop short anthers and defective tapetal cells, and exhibit temperature-sensitive male fertility. We propose that DCL5 and 24-nt phasiRNAs are critical for fertility under growth regimes for optimal yield.

Introduction

Three major classes of endogenous small RNAs (sRNAs) exist in plants: microRNAs (miRNAs), heterochromatic small interfering RNAs (hc-siRNAs), and phased, secondary small interfering RNAs (phasiRNAs). From extensive sRNA sequencing in plants, numerous loci generating phasiRNAs have been reported; in grasses, phasiRNAs are enriched in flowers, particularly male reproductive organs [1–4]. PhasiRNA production is initiated by miRNA-mediated cleavage of RNA polymerase II transcripts of two classes of *PHAS* loci. Subsequently, the 3' portion of cleaved transcripts is converted to double-stranded RNA, a substrate for precise chopping by DICER-LIKE 4 (DCL4) yielding 21-nt products; a distinct, proposed role for DCL5 is in

the generation of 24-nt phasiRNAs [2–4]. The 21-nt phasiRNAs are highly abundant during initial cell fate setting in maize anthers [1] and are important for male fertility in rice [5,6]. The 24-nt phasiRNAs accumulate coincident with meiotic start, peak during meiosis, and persist at lower levels afterwards; this pattern has generated speculation that they regulate meiosis [7,8].

In angiosperms, five DCLs have been described and partially characterized [9]. DCL1 is important for miRNA biogenesis, as illustrated by regulation of meristem determinacy in maize inflorescences [10]. In *Arabidopsis thaliana*, DCL2 processes viral- and transgene-derived siRNAs [11]; DCL3 produces 24-nt hc-siRNAs, which then direct DNA methylation of target loci [12]. In many plants including *Oryza sativa* (rice), DCL4 generates 21-nt *trans*-acting siRNAs and phasiRNAs [3]. Although the functions of these four *DICER-LIKE* genes are well conserved in flowering plants, these genes have partially overlapping functions [11,13]. A fifth, more recently discovered gene, *Dcl5*, is monocot-specific [9]. To better understand the function of DCL5 and its proposed role in 24-nt phasiRNA biogenesis [1], we characterized maize *dcl5* mutants generated using a high efficiency CRISPR-mediated gene editing system [14].

Results

Loss-of-function mutants of the maize *Dcl5* gene confer male-sterility

We picked four alleles for analysis (Fig. 1A), and from T_0 plants we developed stable lines that show Mendelian inheritance of each *dcl5* allele (Fig. 1B, Table S1, and Fig. S1). *dcl5-1* and *dcl5-4* are frameshift mutants with transcript levels down-regulated

47 to about a third of their wild type siblings; in contrast, *dcl5-2* (3 bp deletion) and *dcl5-3*
48 (12 bp deletion, 1 bp substitution) have similar or higher transcript levels compared to
49 control siblings (Fig. 1B and Fig. S2). Wild type and heterozygous *dcl5-1//Dcl5* plants
50 greenhouse-grown at 32° C maximum day/21° C minimum night were identical in whole
51 plant architecture, anther morphology, and fertility. Under the same conditions,
52 homozygous *dcl5-1* plants were male sterile (Fig. 1C). Compared to their fertile siblings,
53 sterile *dcl5-1* plants lacked visible differences in tassels and spikelets, however, the
54 sterile anthers were shorter, contained shrunken pollen, and did not exert from the
55 spikelets (Fig. 1C and Fig. S3). Sporadically, a few anthers exerted and shed viable
56 pollen. Under field conditions, all four alleles showed equivalent levels of male sterility.
57 No genomic editing can be detected in the homologous sequence in *Dcl3* which is the
58 most likely potentially off-target locus (Fig. S4). We concluded that *Dcl5* is required for
59 robust male fertility.
60
61 *dcl5-1* mutants exhibit tapetal defects
62 To investigate whether *dcl5-1* plants display defects in anther cell patterning, we
63 used confocal microscopy and found normal somatic layer architecture without defects in
64 initial cell differentiation (Fig. S5). In addition, chromosome pairing, alignment, and
65 meiotic progression were normal in *dcl5-1* meiocytes (Fig. S6). The *dcl5-1* meiocytes
66 routinely complete meiosis and produce haploid gametophytes. Transmission electron
67 microscopy was utilized to visualize nuclei and other cell organelles at higher resolution.
68 During mid-meiosis (2 to 2.5 mm anthers), normal tapetal cells were densely packed with
69 dark-staining materials and were mostly binucleate (Fig. 2A and Fig. S7). In contrast, the

tapetal cells in *dcl5-1* were pale and mostly mononucleate, and many cell organelles were not clearly resolved (Fig. 2B and Fig. S7). Whole mount, fluorescence microscopy was used to quantify binucleate status in *dcl5-1* and fertile anthers. In 1.5 mm anthers (prophase I), there were five-fold fewer binucleate tapetal cells in *dcl5-1*, and a significant difference persisted at 2.5 mm (meiosis II) (Fig. 2 and Fig. S8). In extensive confocal microscopic examination of *dcl5-1* anthers, we observed no significant or consistent differences in cell number or volume compared to fertile siblings. Collectively, these observations indicate that tapetal development is delayed or arrested and that the *dcl5-1* tapetal cells are therefore likely defective in conducting post-meiotic functions supporting pollen maturation.

Dcl5 is exclusively expressed in the meiocytes and tapetal cells at the onset of meiosis

To obtain a comprehensive spatiotemporal profile of maize *Dcl5* expression, we queried microarray, published and newly generated RNA-seq (Table S2), and proteomics data. *Dcl5* transcripts are highly enriched in tassels, cobs, embryos, and seeds [15,16], and in fertile anthers. In contrast, DCL5 protein is low in 1.0 mm, pre-meiotic anthers and extremely high in 2.0 mm mid-meiosis anthers, but is undetectable in ear, embryo, or endosperm [17]. Microarray analysis of laser-microdissected anther cell types [18,19] and *in situ* hybridization analysis of anther lobes [1,20] established that *Dcl5* transcripts are highly enriched in the tapetum and are present at lower levels in pre-meiotic pollen mother cells and meiocytes. RNA-seq confirmed *Dcl5* expression in isolated maize meiocytes, however, quantitatively there are even higher levels in whole anthers [21], as confirmed by newly-generated anther data (Table S2). Therefore, *Dcl5* is expressed much more highly

93 in one or more somatic cell types than in meiocytes [21]. Integrating prior observations that
94 24-nt phasiRNA biogenesis is contingent on a normal tapetum [1], with the peak of *Dcl5*
95 and DCL5 expression in meiotic anthers, we conclude that the 24-nt phasiRNA pathway
96 is localized in tapetal cells. We hypothesize that this localization and timing is of
97 functional importance for the redifferentiation of tapetal cells into secretory cells.
98
99 24-phasiRNAs abundance is greatly reduced in *dcl5* mutants. To investigate if 24-
100 nt phasiRNA biogenesis is affected in *dcl5* mutants, sRNA libraries were constructed
101 from anthers or spikelets of each *dcl5* allele (Table S2). Previously, we found that 24-nt
102 phasiRNAs were readily detected from 176 24-*PHAS* loci in W23 inbred anthers [1]. The
103 24-nt sRNAs produced from all these loci were reduced dramatically in plants
104 homozygous for each *dcl5* allele compared to fertile siblings even though *dcl5-2* and
105 *dcl5-3* encode proteins that lack only a few amino acids (Fig. 3). Other sRNAs, including
106 24-nt hc-siRNAs and 21-nt phasiRNAs were retained (Fig. S9). We conclude that *Dcl5* is
107 required for 24-nt phasiRNA biogenesis and that the *dcl5-2* and *dcl5-3* mutations define
108 amino acids essential for DCL5 function. Analysis of *24-PHAS* precursors in RNA-seq
109 anther libraries from the same plants showed greater or nearly the same levels of
110 precursor abundance in each of the *dcl5* mutant alleles *4* (Fig. S10). Therefore, the
111 absence of functional DCL5 severely disrupts 24-nt phasiRNA precursor processing with
112 a modest impact on their accumulation.
113
114 Analysis of these RNA-seq data to characterize downstream transcriptional
115 pathways impacted in *dcl5* mutants was uninformative, consistent with prior results that

failed to identify mRNA targets for 24-nt phasiRNAs [1]. The transcriptional changes in *dcl5-1* mutants were minimal with many of these impacted transcripts being downstream effects of the arrested tapetal development (Table S3) and proximal genes were not impacted; alterations in the transcript population are likely indirect and reflective of defective tapetal development.

dcl5-1 mutants are temperature-sensitive male sterile

dcl5-1 field-grown plants exhibited variable fertility under typical summer conditions in Stanford, CA: 25/18° C interrupted by multi-day heat waves exceeding 32° C. To test whether temperature is a restrictive condition, three controlled greenhouse regimes were chosen -- 28/22° C, 26/20° C, and 23/20° C (14 h day/10 h night temperature) -- and maintained within narrow limits over the life cycle (Fig. 4). At 28/22° C, *dcl5-1* mutants had shorter anthers that never exerted, while heterozygous siblings developed normally. In contrast, under both the 26/20° C and 23/20° C regimes, *dcl5-1* mutants were partially to fully fertile; pollen was viable based on Alexander staining despite a prolonged life cycle and delayed flowering date under cooler temperatures (Fig. S11). We also compared *dcl5-1* transcript levels, 24-nt phasiRNA production, and *PHAS* precursor accumulation in *dcl5-1* plants under restrictive and permissive temperature and we observed no significant differences (Fig. 3, Fig. S2 and Fig. S10). Our interpretation is that the functions of *Dcl5* and 24-nt phasiRNAs are dispensable for maize male fertility at low temperatures (23/20° C) but are required at higher temperatures. Cool temperatures slow the pace of development and may allow alternative pathways independent of the 24-nt phasiRNAs to support tapetal cell redifferentiation.

Maize tassels contain anthers representing six days of development [22], and we wondered if sporadic anther exertion in *dcl5-1* plants reflected a short phenocritical period when some anthers experienced permissive conditions. Homozygous *dcl5-1* plants were greenhouse-grown at 28/22° C until the tassel inflorescence formed (~30 days), then plants were moved into two walk-in chambers: permissive 23/20° C or restrictive 28/22° C regimes. In the next three weeks, 14 sets of three plants were swapped between the two regimes for 3, 6, 9, 12, 15, 18 or 21 days, and then all plants finished their life cycle in the 28/22° C greenhouse (Fig. S12). Plants in the 23/20° C regime from the start of meiosis through the release of mononucleate microspores (~9 day period, swaps 7 to 11, Fig. S12) were fully fertile. Sample plants were assessed during the 6th through 9th days to check anther staging in the main tassel spike, confirming that this interval corresponds to meiosis and post-meiotic stages in the most mature part of the tassel. These stages also encompass the initiation, peak, and continued presence of 24-nt phasiRNAs in normal anthers [1]. Plants in the permissive temperature for fewer than nine days during this interval had reduced fertility; we hypothesize that this extended interval is required to allow all anthers to proceed through the phenocritical period to ensure full fertility. The temperature swap experiment demonstrates that there is a short period in which DCL5 is required to "buffer" development at elevated temperatures. Surprisingly, the restrictive temperature is similar to what is considered optimal day temperature for the U.S. corn belt; historical data indicate that growth between 20° to 29° C generates optimal yield, with higher yields associated with warmer temperatures within this range [23,24].

Discussion

Maize DCL5 is essential for robust male fertility: *dcl5* plants are temperature-sensitive during meiosis, show arrested tapetal development at this stage, and lack 24-nt phasiRNAs. In rice, perturbed 21-nt, premeiotic phasiRNAs confer photoperiod and temperature-sensitive male fertility [25–27]. Molecular and *in situ* analyses indicate that the 24-nt phasiRNA biogenesis factors and these sRNAs are located primarily in the tapetum [1]. For maize, we conclude that 24-nt phasiRNAs play a direct role in tapetal redifferentiation and only an indirect role in meiocytes or gametophytes. We hypothesize that the 24-nt phasiRNAs are essential for tapetal redifferentiation for biosynthesis and secretion of materials that support haploid microgametophytes. The molecular mechanisms by which 21- and 24-nt reproductive phasiRNAs act remain unclear.

Our study in maize establishes that DCL5 plays a unique role, having subfunctionalized from DCL3 for 24-nt phasiRNA biogenesis in anthers. *Dcl5* transcripts are still expressed in diverse organs, however, protein and critical functions are restricted to anthers. Expression analysis found just 23 genes differentially expressed in our *dcl5-1* mutants, but all of these are likely reflective of arrested tapetal development. That the thousands of 24-nt phasiRNAs fail to impact mRNA abundances significantly indicates that 24-nt phasiRNAs are distinct from tasiRNAs which do have specific mRNA targets and modulate transcript abundances. DCL5 and therefore the 24-nt phasiRNAs are dispensable at cool growing temperatures for maize, however, DCL5 is required for robust fertility at temperatures for optimal yield in the U.S. corn belt. As climate disruption, including more extensive heat waves, and a general warming trend increase

185 field temperatures, buffering maize tapetal development from adverse effects may be
186 possible by enhancing 24-nt phasiRNA functions. The 24-nt phasiRNAs may permit
187 development during other untested environmental challenges. Given the high degree of
188 variation typically observed across maize inbreds for many traits, the *dcl5* mutant
189 phenotype may vary across inbreds. More generally, it is unknown how many crop plants
190 utilize reproductive phasiRNAs and whether their tapetal health and functions could
191 benefit by introduction or optimization of these or other sRNA pathways [28–30].
192
193 **Materials and Methods**
194 gRNA construction and transformation
195 To increase the mutagenesis frequency in the targeted region, two target sites
196 separated by 76 bp were selected for guide RNA (gRNA) construction, designed using
197 the CRISPR Genome Analysis Tool as previously described [14]. Rice *U6* small nuclear
198 RNA gene promoters (P*U6.1* and P*U6.2*) were used to drive the expression of each
199 gRNA. Guide RNAs were first cloned into a pENTR vector using *Btg*ZI and *Bsa*I (New
200 England BioLabs) restriction enzymes. These constructs were transferred using Gateway
201 recombination to the binary vector containing the *Cas9* gene driven by the maize
202 *Ubiquitin 1* promoter and the *bar* gene driven by *35S* promoter [14]. The final construct was
203 transformed into *Agrobacterium tumefaciens* for delivery into HiII maize immature
204 embryos, followed by screening of positive calli as previously described [14].
205
206 Characterization of transformants

207 DNA samples were extracted from Basta®-resistant calli and screened for
208 mutations in the target region by PCR using primers *Dcl5*_F1 (5'-
209 ATCTAGATCTCCAGACCATTGAACCCTGTC-3') and *Dcl5*_R1 (5'-
210 GTATTCTAGACTTGAATAACCTGCTCTTTG-3'). Positive calli were transferred to
211 regeneration media; multiple plants regenerated from the same callus were considered to
212 be biological clones [14]. No chimeric plants were detected, consistent with Cas9 action in a
213 single cell. Leaves from mature T_0 plants were genotyped for a second time using PCR
214 amplification and Sanger sequencing to confirm the mutations. Over several generations
215 families were established that segregated 1:1 for *dcl5*//+ fertile: *dcl5//dcl5* homozygous
216 sterile individuals using standard maize genetic procedures.

217

218 Microscopy and imaging

219 For anther wall structure analysis with confocal microscopy, the anthers of
220 precisely measured sizes were dissected and stored in 70% ethanol for fixation. Fixed
221 anthers were then stained by propidium iodide and visualized on a Leica SP8 confocal
222 microscope as previously described [18]. Meiocytes were extruded and stained by DAPI
223 (4',6-diamindino-2-phenylindole) following published protocols [31]. The Alexander's
224 staining solution [32] was used to test the viability of the pollen grains in the permissive
225 conditions. TEM procedures were followed as described [33], summarized as follows:
226 anthers were dissected and fixed in fresh 0.1 M PIPES buffer (pH 6.8). A 2% osmium
227 tetroxide stain was applied with brief washes, followed by dehydration in an acetone
228 gradient. Specimens were infiltrated using a gradient of Spurr's resin (Sigma-Aldrich)
229 and embedded. The sections were cut using a Leica UCT ultramicrotome, stained in urayl

and lead salts, and observed using a Zeiss TEM instrument with a LEO 912 AB energy filter.

ScaleP clearing of maize anthers

Maize anthers were fixed directly into 4% paraformaldehyde in phosphate-buffered saline (pH 7.4), and then prepared following the ScaleP protocol [34]. After 8 h KOH treatment, anthers were stained for a week at room temperature with 1 mM Calcofluor white for imaging of cell walls and 5 µM Syto13 (ThermoFisher) for imaging nuclei. Samples were then cleared for three days with ScaleP solution consisting of 6 M urea, 30% (v/v) glycerol, and 0.1% (v/v) Triton X-100 in sterile water. Cleared samples were then imaged with a Zeiss 880 multi photon confocal microscope with a 40× LD C-Apochromat water lens (numerical aperture of 1.1; working distance of 0.62 mm). The 3D rendering was performed with Amira (FEI, ThermoFisher) software. Tapetal cells were classified as mononucleate or binucleate, and then artificially colored.

sRNA-seq and RNA-seq library construction and sequencing

Total RNA for sRNA-seq and RNA-seq libraries was isolated using the PureLink Plant RNA Reagent (ThermoFisher) following the manufacturer's instructions. Total RNA quality was assessed by denaturing agarose gel electrophoresis and quantified by the Qubit RNA BR Assay Kit (ThermoFisher). For library preparation, 20 to 30 nt RNAs were excised from a 15% polyacrylamide/urea gel, and ~25 ng of sRNA used for library construction with the TruSeq Small RNA Prep Kit (Illumina) following the

252 manufacturer's instructions. For RNA-seq, 2 µg of total RNA was treated with DNase I
253 (New England BioLabs) and then cleaned with RNA Clean and Concentrator-5 (Zymo
254 Research). The TruSeq Stranded Total RNA with RiboZero-Plant Kit (Illumina) was used
255 for library construction with 500 ng of treated RNA, following the manufacturer's
256 instructions. Sequencing in single-end mode on an Illumina HiSeq 2500 (University of
257 Delaware) yielded 51 bp reads for both sRNA-seq and RNA-seq.

258

259 sRNA-seq data were processed as previously described [35]. Briefly, we first used
260 Trimmomatic version 0.32 to remove the linker adaptor sequences [36]. The trimmed reads
261 were then mapped to version 4 of the B73 maize genome using Bowtie [37]. Read counts
262 were normalized to 20 million to allow for the direct comparison across libraries.
263 phasiRNAs were designated based on a 24-nt length and mapping coordinates within the
264 previously identified 176 *24-PHAS* loci [1], updated to version 4 of the B73 genome using
265 the assembly converter tool [38]. If a 24-nt phasiRNA did not uniquely map to the genome,
266 we divided the abundance equally to each location to which the read mapped, i.e. a hits-
267 normalized abundance. These hits-normalized abundances were then summed for each of
268 the 176 loci to calculate the 24-nt phasiRNA abundances.

269

270 RNA-seq libraries were trimmed as above, and mapped to version 4 of the B73
271 genome using Tophat version 2.0.12 [39]. For differential expression analysis of genes, we
272 assembled the transcripts using the Cufflinks package [40] and raw gene expression levels
273 were quantified using featureCounts version 1.5.0 [41] to generate count tables that were
274 imported into R for statistical analysis [42]. Weakly expressed transcripts (fewer than 1

read) were filtered out, and the remaining transcripts were normalized using DEseq2 to finally identify a set of differentially expressed genes for anthers homozygous for each mutant allele [43]. Due to a lack of a replicate for the *dcl5-1* restrictive library, we calculated dispersions using the mean of libraries to identify differentially expressed transcripts without a complete set of replicates.

For differential expression analysis of the *PHAS* precursors, we were unable to assemble the transcripts that mapped to these regions because of the absence of annotation in any feature files. Instead, we conducted this analysis in parallel to the analysis of the sRNA data. We first normalized the mapped fragmented reads as counts per 15 million, and applied the hits-normalized abundance approach described above. Using the annotated *24-PHAS* loci (above), we then identified the summed abundance of RNA-seq transcript fragments that mapped to these regions to identify a representative abundance for each *24-PHAS* precursor. Replicate libraries were averaged together prior to the creation of the heatmap, and we added 1 to all abundances in order to prevent $\log_2(0)$ error while also giving the added benefit of removing negative log transformed values. Boxplots were generated for each replicate's log transformed values.

References

1. Zhai, J. *et al.* Spatiotemporally dynamic, cell-type–dependent premeiotic and meiotic phasiRNAs in maize anthers. *Proc. Natl. Acad. Sci.* ***112*****,** 3146–3151 (2015).

2. Johnson, C. *et al.* Clusters and superclusters of phased small RNAs in the developing inflorescence of rice. *Genome Res.* ***19*****,** 1429–1440 (2009).

3. Song, X. *et al.* Roles of DCL4 and DCL3b in rice phased small RNA biogenesis. *Plant J.* ***69*****,** 462–474 (2012).

4. Song, X. *et al.* Rice RNA-dependent RNA polymerase 6 acts in small RNA biogenesis and spikelet development. *Plant J.* ***71*****,** 378–389 (2012).

5. Nonomura, K.-I. *et al.* A germ cell specific gene of the *ARGONAUTE* family is essential for the progression of premeiotic mitosis and meiosis during sporogenesis in rice. *Plant Cell* ***19*****,** 2583–94 (2007).

6. Komiya, R. *et al.* Rice germline-specific Argonaute MEL1 protein binds to phasiRNAs generated from more than 700 lincRNAs. *Plant J.* ***78*****,** 385–397 (2014).

7. Nonomura, K.-I. Small RNA pathways responsible for non-cell-autonomous regulation of plant reproduction. *Plant Reprod.* ***31*****,** 21–29 (2018).

8. Ono, S. *et al.* EAT1 transcription factor, a non-cell-autonomous regulator of pollen production, activates meiotic small RNA biogenesis in rice anther tapetum. *PLOS Genet.* ***14*****,** e1007238 (2018).

9. Margis, R. *et al.* The evolution and diversification of Dicers in plants. *FEBS Lett.* ***580*****,** 2442–2450 (2006).

10. Thompson, B. E. *et al.* The *dicer-like1* homolog *fuzzy tassel* is required for the regulation of meristem determinacy in the inflorescence and vegetative growth in maize. *Plant Cell* ***26*****,** 4702–17 (2014).

11. Parent, J. S., Bouteiller, N., Elmayan, T. & Vaucheret, H. Respective contributions of Arabidopsis DCL2 and DCL4 to RNA silencing. *Plant J.* ***81*****,** 223–232 (2015).

12. Daxinger, L. *et al.* A stepwise pathway for biogenesis of 24-nt secondary siRNAs and spreading of DNA methylation. *EMBO J.* ***28*****,** 48–57 (2009).

13. Gasciolli, V., Mallory, A. C., Bartel, D. P. & Vaucheret, H. Partially redundant functions of Arabidopsis DICER-like enzymes and a role for DCL4 in producing trans-acting siRNAs. *Curr. Biol.* ***15*****,** 1494–1500 (2005).

14. Char, S. N. *et al.* An Agrobacterium-delivered CRISPR/Cas9 system for high-frequency targeted mutagenesis in maize. *Plant Biotechnol. J.* ***15*****,** 257–268 (2017).

15. Sekhon, R. S. *et al.* Genome-wide atlas of transcription during maize development. *Plant J.* ***66*****,** 553–563 (2011).

16. Stelpflug, S. C. *et al.* An expanded maize gene expression atlas based on RNA sequencing and its use to explore root development. *Plant Genome* ***9*****,** doi:10.3835/plantgenome2015.04.0025 (2016).

17. Walley, J. W. *et al.* Integration of omic networks in a developmental atlas of maize. *Science* ***353*****,** 814–818 (2016).

18. Zhang, H. *et al.* Transcriptomes and proteomes define gene expression progression in pre-meiotic maize anthers. *G3* ***4*****,** 993–1010 (2014).

19. Kelliher, T. & Walbot, V. Maize germinal cell initials accommodate hypoxia and precociously express meiotic genes. *Plant J.* ***77*****,** 639–652 (2014).

20. Nan, G.-L. *et al.* MS23, a master basica helix-loop-helix factor, regulates the specification and development of tapetum in maize. *Development* ***144*****,** 163–172 (2017).

21. Dukowic-Schulze, S. *et al.* Novel meiotic miRNAs and indications for a role of phasiRNAs in meiosis. *Front. Plant Sci.* ***7*****,** 762 (2016).

22. Egger, R. L. & Walbot, V. Quantifying *Zea mays* L tassel development and correlation with anther developmental stages as a guide for experimental studies. *Maydica* ***60*****,** (2015).

23. Schlenker, W. & Roberts, M. J. Nonlinear effects of weather on corn yields. *Rev. Agric. Econ.* ***28*****,** 391–398 (2006).

24. Schlenker, W. & Roberts, M. J. Nonlinear temperature effects indicate severe damages to U.S. crop yields under climate change. *Proc. Natl. Acad. Sci.* ***106*****,** 15594–15598 (2009).

25. Zhou, H. *et al.* Photoperiod- and thermo-sensitive genic male sterility in rice are caused by a point mutation in a novel noncoding RNA that produces a small RNA. *Cell Res.* ***22*****,** 649–660 (2012).

26. Fan, Y. *et al.* PMS1T, producing phased small-interfering RNAs, regulates photoperiod-sensitive male sterility in rice. *Proc. Natl. Acad. Sci.* ***113*****,** 15144–15149 (2016).

27. Ding, J. *et al.* A long noncoding RNA regulates photoperiod-sensitive male sterility, an essential component of hybrid rice. *Proc. Natl. Acad. Sci.* ***109*****,** 2654–2659 (2012).

28. Vernoud, V. *et al.* The HD-ZIP IV transcription factor OCL4 is necessary for trichome patterning and anther development in maize. *Plant J.* ***59*****,** 883–894 (2009).

29. Yu, J. *et al.* Two rice receptor-like kinases maintain male fertility under changing temperatures. *Proc. Natl. Acad. Sci.* ***114***, 12327-12332 (2017).

30. Storme, N. D. & Geelen, D. The impact of environmental stress on male reproductive development in plants: biological processes and molecular mechanisms. *Plant Cell Environ.* ***37*****,** 1–18 (2014).

366 31. Zhang, H. *et al.* Stable integration of an engineered megabase repeat array into the
367 maize genome. *Plant J.* ***70*****,** 357–365 (2012).
368 32. Alexander, M. P. Differential staining of aborted and nonaborted pollen. *Biotech.*
369 *Histochem.* ***44*****,** 117–122 (1969).
370 33. Wang, L. *et al.* Characterization and fine mapping of a necrotic leaf mutant in maize
371 (*Zea mays* L.). *J. Genet. Genomics* ***40*****,** 307–314 (2013).
372 34. Warner, C. A. *et al.* An optical clearing technique for plant tissues allowing deep
373 imaging and compatible with fluorescence microscopy. *Plant Physiol.* ***166*****,** 1684–
374 1687 (2014).
375 35. Mathioni, S. M., Kakrana, A. & Meyers, B. C. Characterization of plant small RNAs
376 by next generation sequencing. *Curr. Protoc. Plant Biol* ***2*****,** 39–63 (2017).
377 36. Bolger, A. M., Lohse, M. & Usadel, B. Trimmomatic: A flexible trimmer for
378 Illumina sequence data. *Bioinformatics* ***30*****,** 2114–2120 (2014).
379 37. Kersey, P. J. *et al.* Ensembl Genomes 2016: more genomes, more complexity.
380 *Nucleic Acids Res.* ***44*****,** D574–D580 (2016).
381 38. Tello-Ruiz, M. K. *et al.* Gramene 2018: Unifying comparative genomics and pathway
382 resources for plant research. *Nucleic Acids Res.* ***46*****,** D1181–D1189 (2018).
383 39. Trapnell, C., Pachter, L. & Salzberg, S. L. TopHat: Discovering splice junctions with
384 RNA-Seq. *Bioinformatics* ***25*****,** 1105–1111 (2009).
385 40. Trapnell, C. *et al.* Transcript assembly and quantification by RNA-Seq reveals
386 unannotated transcripts and isoform switching during cell differentiation. *Nat.*
387 *Biotechnol.* ***28*****,** 511–515 (2010).

388 41. Liao, Y., Smyth, G. K. & Shi, W. FeatureCounts: An efficient general purpose
389 program for assigning sequence reads to genomic features. *Bioinformatics* ***30*****,** 923–
390 930 (2014).
391 42. R Development Core Team. *R: A language and environment for statistical*
392 *computing. R Foundation for Statistical Computing* ***1*** (2011).
393 43. Love, M. I., Huber, W. & Anders, S. Moderated estimation of fold change and
394 dispersion for RNA-seq data with DESeq2. *Genome Biol.* ***15*****,** 550 (2014).
395

396 **Acknowledgments**

397 The *dcl5* CRISPR mutants were generously generated by Dr. Bing Yang's group
398 at Iowa State University. TEM images were produced and imaged by Dr. Howard Berg at
399 the Donald Danforth Plant Science Center. We thank the greenhouse staff at the Donald
400 Danforth Plant Science Center for facilitating the temperature swap experiment, Sandra
401 Mathioni for the preparation of small RNA and RNA-seq libraries, and Jeff Caplan for
402 advice on microscopy. **Funding:** This work was supported by U.S. National Science
403 Foundation Plant Genome Research Program (NSF-PGRP) award #1649424. Author
404 contributions: H.Z., B.C.M, and V.W. conceived of the project, H.Z., C.T., and K.H.
405 performed and interpreted experiments, R.Z. analyzed sequencing data, H.Z. and C.T.
406 wrote the manuscript with editing by V.W., B.C.M, and with input from all co-authors.
407 **Competing Interests:** V.W. and B.C.M declare that a patent application was filed
408 concerning the use of *Dcl5* for modulating male fertility. **Data and materials**
409 **availability:** Correspondence and requests for materials should be addressed to
410 walbot@stanford.edu. Raw data were submitted to GEO under GSE122449 (including

411 sRNA-seq as GSM3466686 to GSM3466700 and RNA-seq data as GSM3466701 to

412 GSM3466714), and the processed data are available via our maize genome browser at

413 https://mpss.danforthcenter.org.

Main Figures

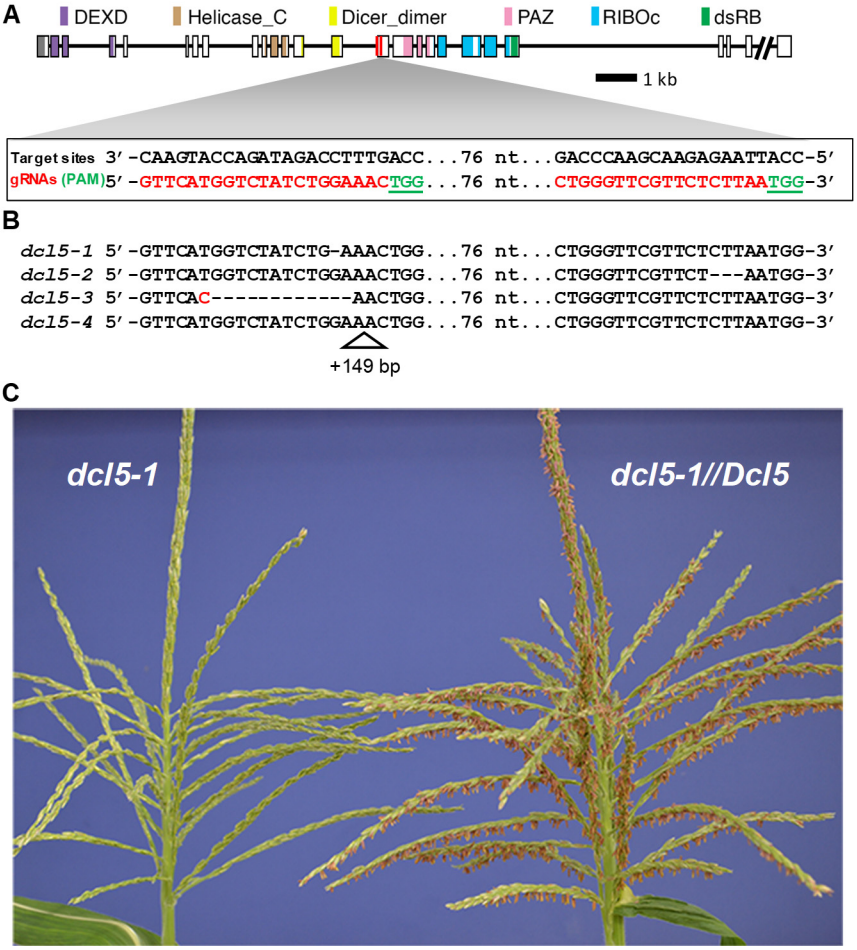

Fig. 1. CRISPR-Cas9 was used in maize to mutate *Dcl5*.

(A) Schematic diagram of the *Dcl5* gene model. Conserved domains were identified using the NCBI conserved domain search tool against database CDD v3.16. All domains were found with extremely high confidence except the double stranded RNA-binding (dsRB) domain, which had an e-value of 0.05. **(B)** Sequence of the four mutant alleles selected for this study. **(C)** A *dcl5-1* tassel lacking any exerted anthers (left) and a sibling heterozygous *dcl5-1//Dcl5* plant at peak pollen shed with hundreds of exerted anthers (right).

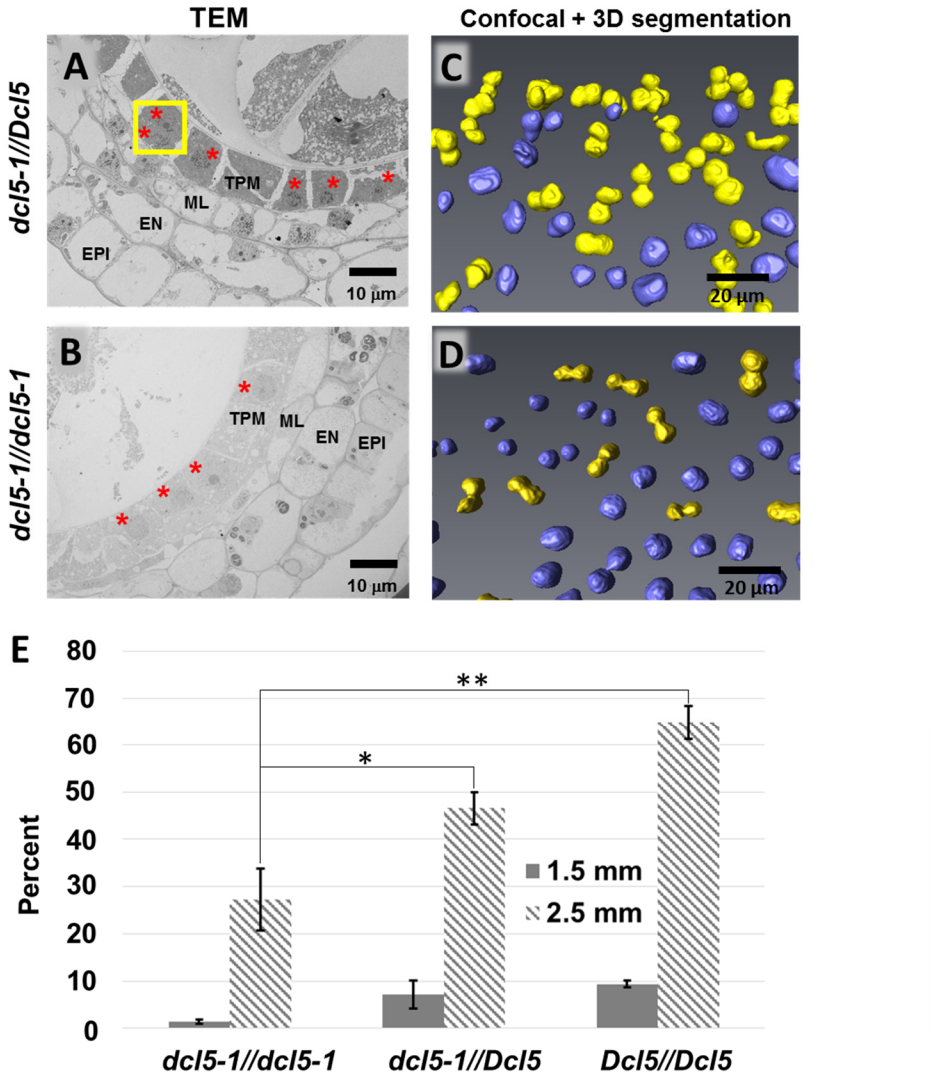

424

425 **Fig. 2. Tapetal cells in *dcl5-1* plants are delayed or arrested in achieving binucleate**

426 **status.**

427 **(A)** Transmission electron microscopy (TEM) of a fertile *dcl5-1//Dcl5* 2 mm anther lobe.

428 At this stage, the tapetal cells (TPM) are packed with dark staining materials, likely exine

429 components later secreted onto haploid microspores. The middle layer (ML), endothecial

430 (EN), and epidermal (EPI) cells are highly vacuolated. The orange boxes mark two

431 binucleate tapetal cells in which both nuclei were visible (red dots). **(B)** TEM of a sterile

432 *dcl5-1* anther lobe at the same stage, demonstrating distended, pale-staining, and

433 mononucleate tapetal cells. **(C)** *dcl5-1*, and **(D)** *dcl5-1//Dcl5:* three-dimensional

434 reconstructions of cleared, 2.5 mm anthers stained with the nuclear marker Syto13.

435 Individual nuclei of mononucleate tapetal cells are marked in purple, and bi-nucleate

436 cells are marked in yellow. **(E)** Quantification of mono- and bi-nucleate cells in *dcl5-1*,

437 *dcl5-1//Dcl5,* and wildtype siblings at the meiotic I (1.5 mm) and meiotic II (2.5 mm)

438 stages, in a family segregating 1:2:1 (*p*-value: $p < 0.05$ *, $p < 0.01$ **)

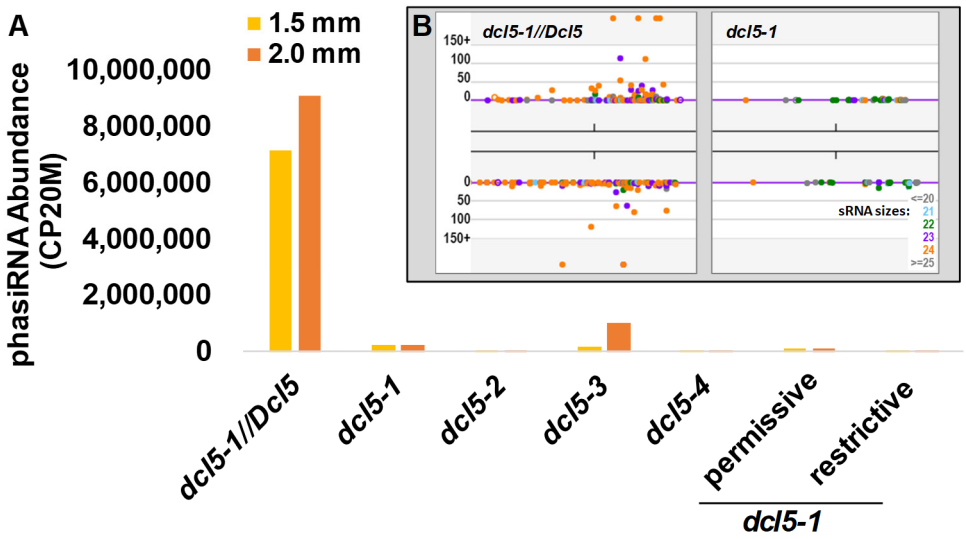

439 **Fig. 3. Near absence of 24-nt phasiRNAs in *dcl5* mutants.**

440 **(A)** Total 24-nt phasiRNAs from 176 *24-PHAS* loci are highly abundant in both 1.5 and

441 2.0 mm fertile heterozygous anthers, and reduced by >99% in abundance in *dcl5-1, dcl5-*

442 *2,* and *dcl5-4*, and by >90% in *dcl5-3* anthers. Altered temperature regimes do not restore

443 24-phasiRNA abundances in either fertile (permissive) or sterile (restrictive) *dcl5-1*

444 anthers (see main text). **(B, inset)** Representative *24-PHAS* locus #12 (B73, v4; chr 1,

445 178454619 bp) in a genome browser showing ~1.5 kbp with sRNAs in the fertile

446 heterozygote (left) and *dcl5-1* (right). Orange dots are individual phasiRNAs; x-axis is

447 genome position on top or bottom strand, y-axis is abundance in each genotype. Other

448 colored dots are as indicated in the key, lower right.

449

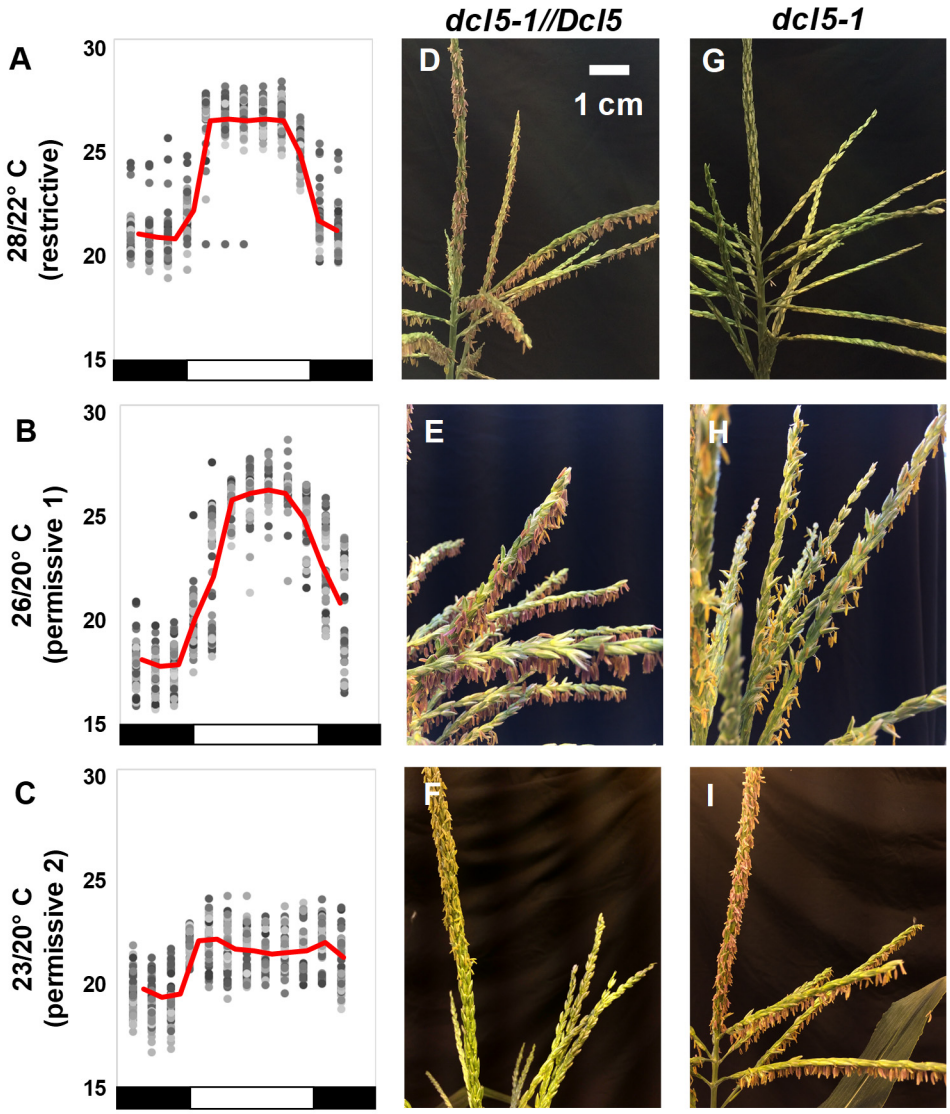

450 **Fig. 4. *dcl5-1* anther fertility is temperature sensitive.**

451 Three sets of *dcl5-1* and sibling *dcl5-1//Dcl5* plants grown in greenhouses with

452 differing temperature regimes: 28°/22° C, 26°/20° C, or 23°/20° C (day/night). **(A, B, C)**

453 Temperatures were recorded every 2 h for 60 days (grey dots, average in red; day/night

454 indicated as white or black, below). **(D, E, F)** Heterozygous *dcl5-1//Dcl5* siblings were

455 fully fertile under all three regimes. **(G, H, I)** *dcl5-1* plants in the restrictive regime **(G)**

456 were completely male sterile, while those in permissive conditions were partially **(H)** or

457 fully **(I)** fertile. Images were taken at 60±3 days after planting (DAP) (top row), 70±2

458 DAP (middle row), and 71±3 DAP (bottom row); the pace of tassel development is

459 temperature-dependent and full anther exertion occurs at different times, for example **(F)**

460 was photographed on the first day of anther exertion, a six-day process. The scale bar in

461 **(A)** is approximate and pertains to all tassel images.